



Embedded Young Stellar Objects near H72.97-69.39: A Forming Super Star Cluster in N79

Om narayani Nayak^{1,2} , Conor Nally³ , Alec S. Hirschauer¹ , Olivia C. Jones⁴ , Jeroen Jaspers^{5,6} , Laura Lenkić^{7,8} , Margaret Meixner⁸ , Nolan Habel^{7,8} , Megan Reiter⁹ , Laurie Chu¹⁰ , Patrick J. Kavanagh⁵ , Massimo Robberto^{1,11} , and B. A. Sargent^{1,11}

¹ Space Telescope Science Institute, 3700 San Martin Drive, Baltimore, MD 21218, USA; omnarayani.nayak@nasa.gov

² NASA Goddard Space Flight Center, 8800 Greenbelt Road, Greenbelt, MD, USA

³ Institute for Astronomy, University of Edinburgh, Blackford Hill, Edinburgh EH9 3HJ, UK

⁴ UK Astronomy Technology Centre, Royal Observatory, Blackford Hill, Edinburgh EH9 3HJ, UK

⁵ Department of Experimental Physics, Maynooth University, Maynooth, Co Kildare, Ireland

⁶ Dublin Institute for Advanced Studies, School of Cosmic Physics, Astronomy & Astrophysics Section, 31 Fitzwilliam Place, Dublin 2, Ireland

⁷ Stratospheric Observatory for Infrared Astronomy, NASA Ames Research Center, Mail Stop 204-14, Moffett Field, CA 94035, USA

⁸ Jet Propulsion Laboratory, California Institute of Technology, 4800 Oak Grove Drive, Pasadena, CA 91109, USA

⁹ Department of Physics & Astronomy, Rice University, 6100 Main Street, Houston, TX 77005, USA

¹⁰ Infrared Processing and Analysis Center, California Institute of Technology, 1200 E California Boulevard, Pasadena, CA 91125, USA

¹¹ Department of Physics & Astronomy, Johns Hopkins University, 3400 N. Charles Street, Baltimore, MD 21218, USA

Received 2024 March 25; revised 2024 August 30; accepted 2024 September 13; published 2024 November 7

Embedded Young Stellar objects near H72.97-69.39: A Forming SSC in N79



The distinct 'starburst' pattern surrounding this bright object is a series of diffraction spikes. All telescopes which use a mirror to collect light, as JWST, present artifact which arises from the design of the telescope. In this case, the six largest starburst spikes appear because of the hexagonal symmetry of Webb's 18 primary mirror segments. Patterns like these are only noticeable around very bright, compact objects.



Infrared 7.7 μm
PAH

F770W

Infrared 10 μm
Silicate

F1000W

Infrared 15 μm

F1500W

Infrared 21 μm

F2100W

Focus: 102 embedded **Young Stellar Objects** (YSOs) candidates observed with James Webb Space Telescope Mid-InfraRed Instrument (MIRI) in four different bands: F700W, F1000W, F1500W, F2100W

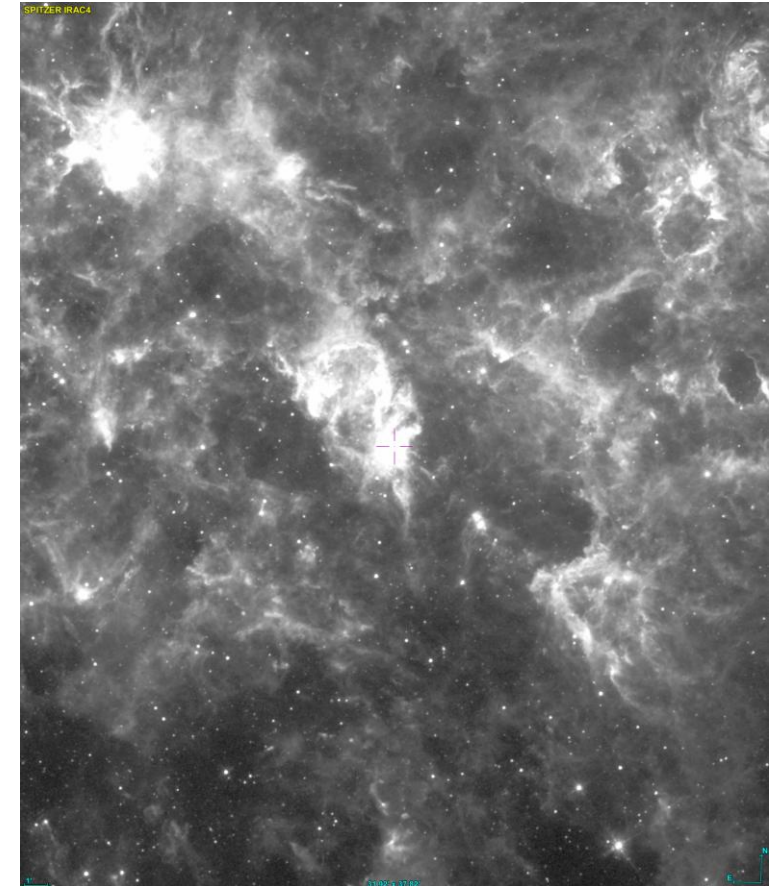
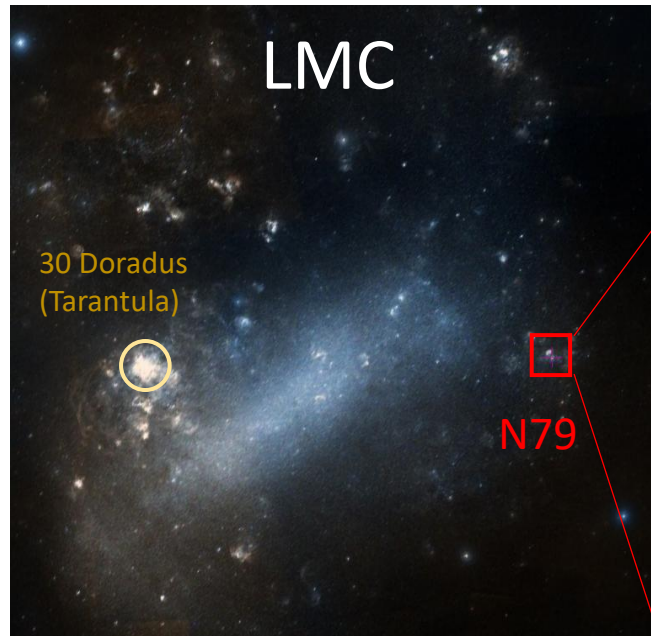
Location: the Giant Molecular Cloud complex **N79** of the Large Magellanic Cloud (LMC)

Methods: Spectro-photometric analysis of multi-band data from JWST data and other instruments (Spitzer)

Aims: Characterize the Super Star Cluster candidate at the center of the star forming region

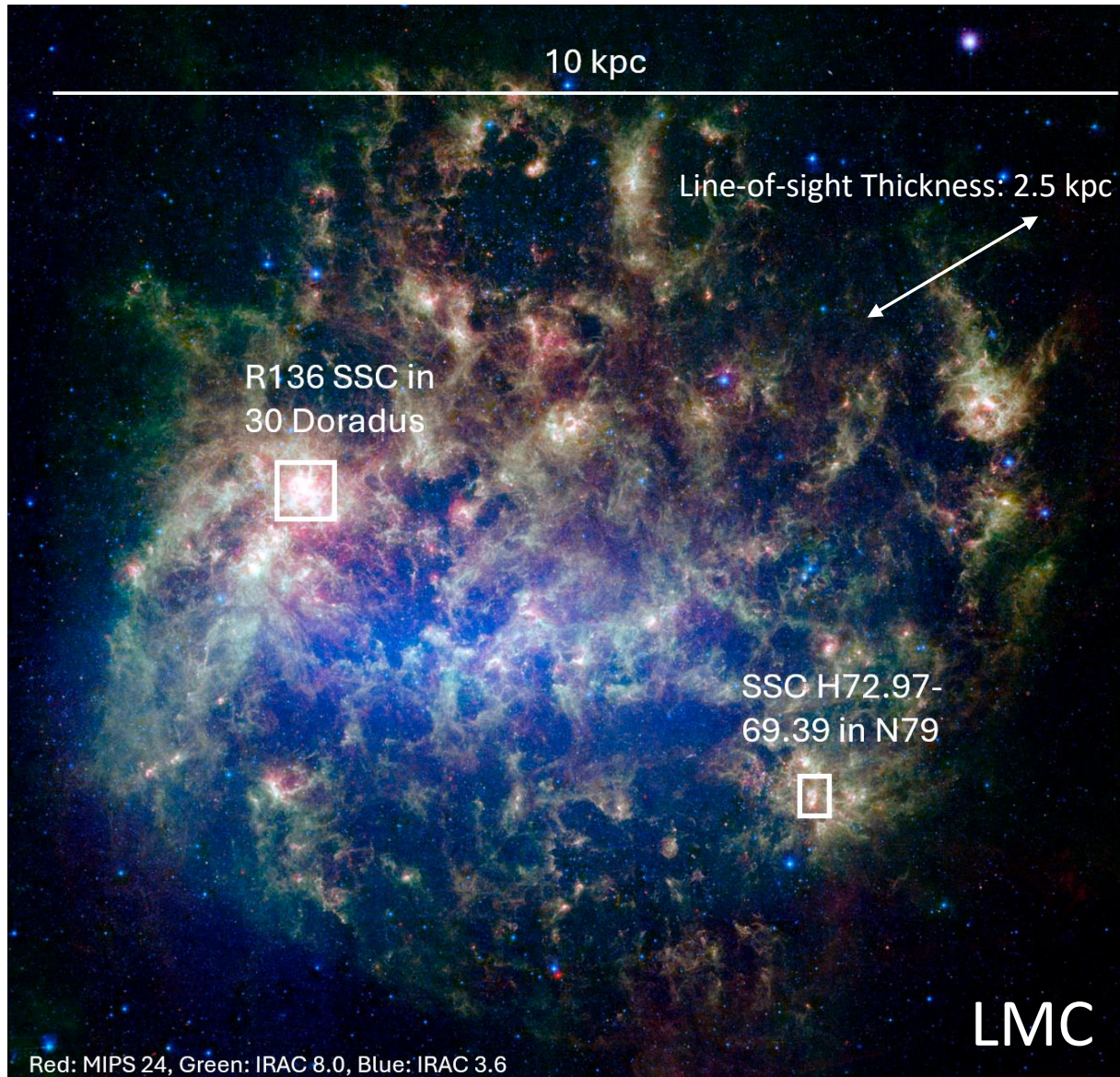
YSO is a general term for a star in its early stages of formation, before it reaches the **main sequence**. YSOs are often embedded in gas and dust and are strong sources of infrared radiation due to the heat from their contraction and accretion processes. They can be roughly divided into two main categories: 1) YSO in protostar phase - deeply embedded, mostly accretion-dominated; 2) Pre-Main Sequence phase – T Tauri stars, surrounded by accretion (protoplanetary) disks

Embedded Young Stellar objects near H72.97-69.39: A Forming SSC in N79



Spitzer (IRAC4: 6.3 μ m – 9.6 μ m)

Embedded Young Stellar objects near H72.97-69.39: A Forming SSC in N79



The LMC lies at about 50 kpc from the Milky Way

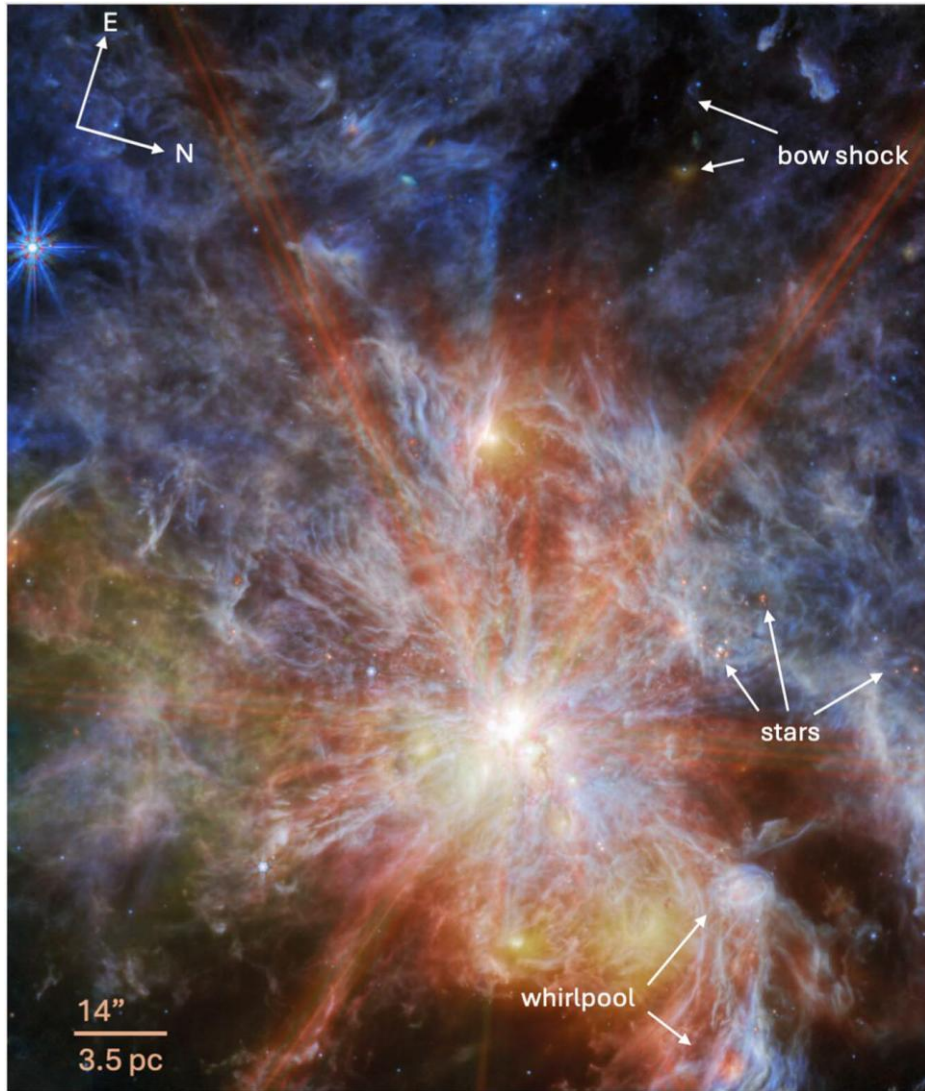
It hosts many of the types of objects like ~ 60 globular clusters and ~ 700 open clusters

The LMC is a site of active star formation: the most notable SFR is 30 Doradus, popularly known as the Tarantula Nebula. This objects contains R136, one of the two massive ($\sim 10^5 M_{\odot}$) SSC present in the LMC, which host the most massive stars ($150-230 M_{\odot}$) known in the Local Universe To give a sense of how impressive the Tarantula Nebula is, consider that if it were as close to us as the Orion Nebula is (about 1,300 lyr), the Tarantula Nebula would appear in our night sky as large as 60 full moons and would be so bright as to cast shadows.

It represents a link between our Galaxy and the Universe (distance ladder...)

The LMC average metallicity is $0.5 Z_{\odot}$ -- it reflects the conditions of star formation present at redshift $z \approx 2$

Embedded Young Stellar objects near H72.97-69.39: A Forming SSC in N79



This composite MIRI image is the result of different exposures covering the entire GMC hosting the candidate SSC. The picture covers an area of about $144'' \times 226''$, corresponding to $36 \text{ pc} \times 57 \text{ pc}$. The FoV shows the presence of protostars, bow shocks, and whirlpool-like emitting structures. Very dusty regions have intense mid-IR flux in yellow (F1500W) and red (F2100W). Small yellow and red dots are young protostars forming within their parental GMC. Several small cluster of stars form cavities, visible as red dots surrounded by blue bubbles, while individual protostars originate bow shocks (arc-like structures), and yellow and cyan hollow regions do not show sign of stellar activity.

At the center lies a very bright object, which is the candidate SSC cluster investigated in this paper. SSCs are so massive, dense ($\sim 1 \text{ pc}$), and tightly bound that the violent star formation occurring in their turbulent, high-pressure, gas-rich environments, allows them to resist gas expulsion by stellar feedback for extended periods ($\sim 100 \text{ Myr}$), enabling exceptionally high star formation efficiencies. They are believed to be the precursors of ancient globular clusters, and as such they play crucial role in shaping galaxies and driving their evolution.

The formation of massive stars significantly changes the thermodynamic state of the interstellar medium (ISM). Massive stars influence their surroundings through radiative and mechanical processes, including stellar winds, supernova explosions, and ultraviolet photo-ionization. This stellar feedback shapes the characteristics of the interstellar medium (ISM) and has dual effects on star formation: it can either suppress the birth of new stars by disrupting developing molecular clouds or enhance it by **helping gravity overcome forces that would otherwise resist cloud collapse**.

Simulations have shown that stellar winds, radiation pressure, photoionization, and gravity of the initial molecular cloud interact with each other. Different mechanisms dominate at different timescales based on metallicity, stellar masses, cluster density, cooling rate of stars, the radiation condition within an H II region, as well as the mass and density of the parental molecular cloud.

1. At the early stages of star formation, bipolar jets and stellar winds inject energy into the surrounding environment. For the first 0.1 Myr, the expansion of an H II region in high-pressure environments is driven by direct radiation from the central protostars. Both stellar wind pressure from the protostar as well as dust-processed radiation pressure equally contribute during the first 1 Myr of growth, while warm ionized gas within the H II region dominates the pressure and expansion after 1 Myr.
2. Radiation pressure drives the HII expansion if the cloud is optically thick, which usually is true during the first 2 - 3 Myr.
3. More massive clouds expand more slowly, and radiation pressure dominates for even longer.
4. Stellar winds more than radiation pressure, play a major role in clouds of $10^5 M_{\odot}$ in size, however the role of stellar winds is less prominent in more massive clouds.
5. At a later stage, massive stars will end in supernova explosions, instantly releasing $\sim 10^{51}$ erg of energy into the ISM, shredding molecular clouds and terminating the local star formation process. Some simulations also show feedback from a supernova explosion is not always sufficient to destroy a molecular cloud. Each feedback mechanism affects the efficiency of others.

Embedded Young Stellar objects near H72.97-69.39: A Forming SSC in N79

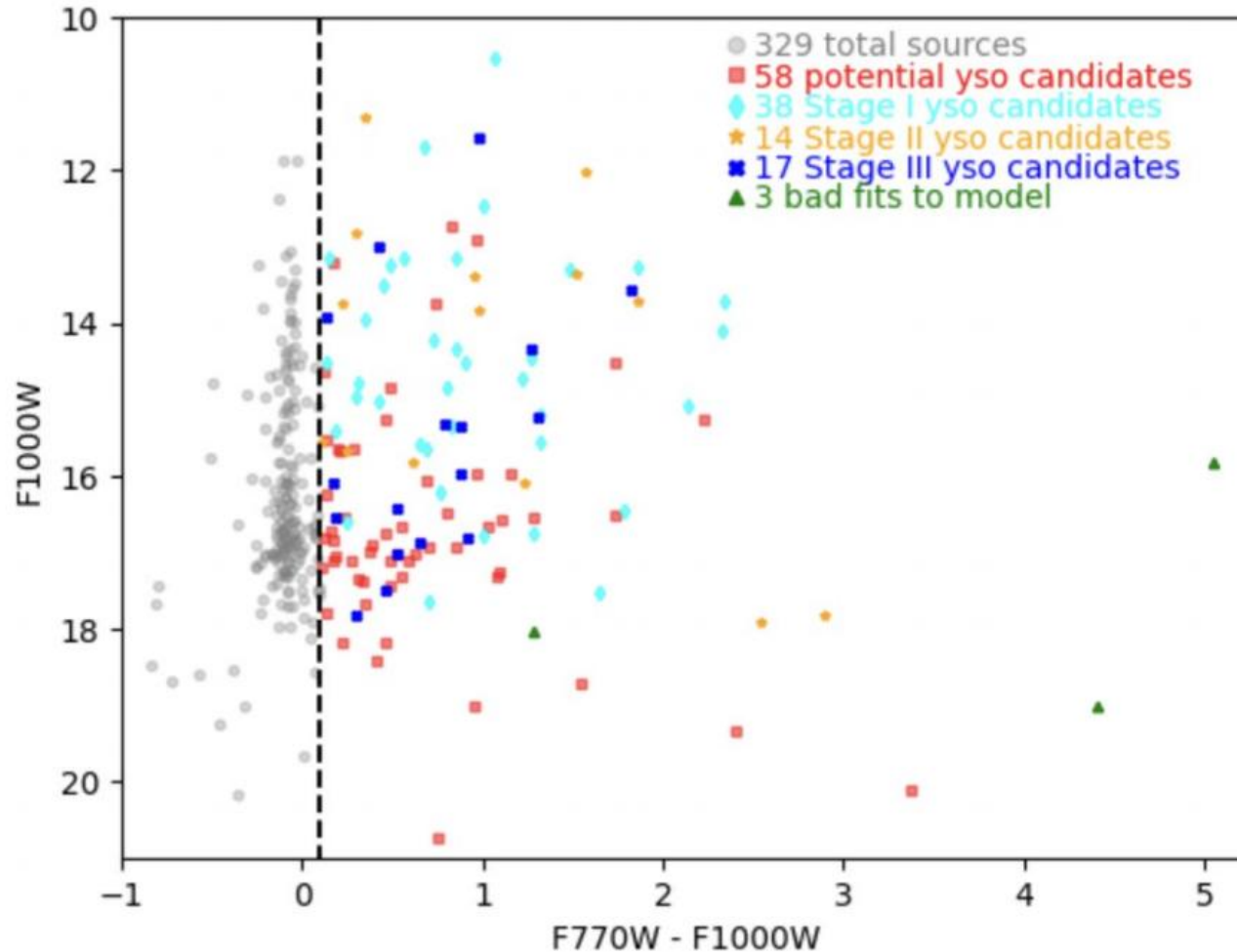


Figure 2. The F700W – F1000W vs. F1000W CMD. There are 133 sources that have $F770W - F1000W > 0.1$; of these 133 sources, 58 have only two photometric points and we are unable to constrain their SEDs, while for the remaining 72 sources, we fit all available photometric points for each sources with model YSO SEDs from T. P. Robitaille (2017). We find three of the 72 red sources do not have well-fit models to the observed data (reduced $\chi^2 > 10$), which we show with green triangles.

The adoption of this CMD for the selection of YSO objects is justified by the fact that previous Spitzer and Herschel observations have shown that the SEDs of young protostars have a steep rise toward the mid- and far-infrared wavelengths, with the youngest and most embedded having a peak around $100\ \mu\text{m}$. There are a total of 329 point sources with a detection in both the F770W and F1000W bands. Since CMDs with other filter combinations have far fewer points, the authors only discuss the F700W – F1000W versus F1000W CMD in this work. They identified sources with zero color (possible main sequence of supergiant stars) and sources which are red (possible YSO candidates). Some sources which are identify as YSO candidates may be evolved stars on the AGB. Indeed AGB stars and bright YSOs occupy a similar space in their CMDs. However, Nayak et al. (2019), used CO outflows associated with H72.97-69.39 to calculate an outflow timescale of 6.5×10^4 yr. This young region is going through its initial star-forming phase and likely has not had sufficient time for a significant number of AGB stars to form.

Stage I consists of sources with an envelope density power between -2 and -1.5 ;
Stage II comprises sources with an envelope density power between -1.5 to -1 and a cavity power of 1.5 – 2 ;
Stage III consists of sources with an envelope density power between -1.5 to -1 and a cavity power of 1 – 1.5

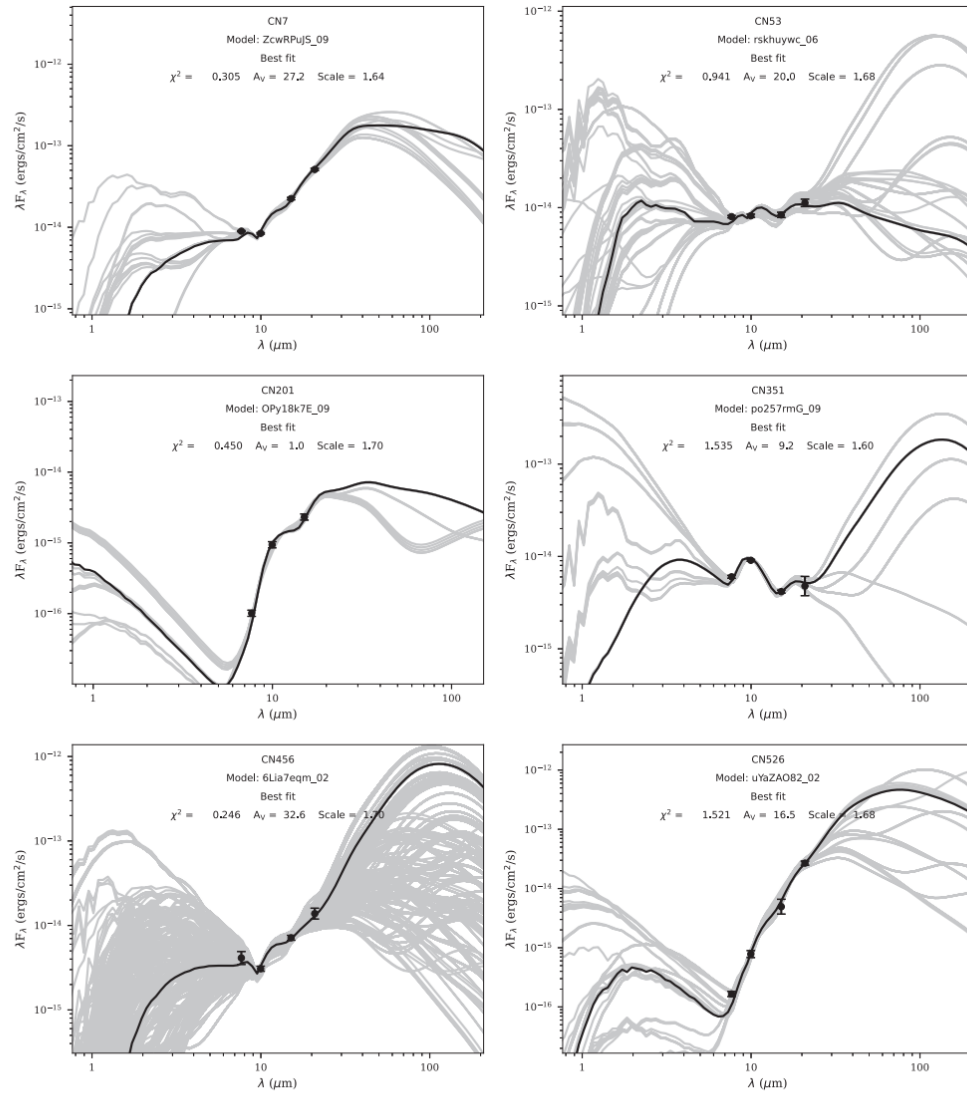


Figure 3. Six YSO candidates fit with T. P. Robitaille (2017) SED models. These are sources with at least three photometric points and within the color cut $F770W - F1000W > 0.5$. The black circles are the observed photometry, the black line is the best-fit model to the observations, and the gray lines are all models with $\Delta\chi^2 < 3$ compared to the best-fit model.

The authors used T. Richardson et al. (2024) SED models (which are the T. P. Robitaille 2017 models convolved with JWST filters) to characterize the properties of the YSO candidates.

The differing grids of models represent a variety of parameters, including: possession of either a passive disk or no disk at all; no envelope, a power-law envelope, or an envelope density structure; cavity or no cavity; ambient medium or no ambient medium; inner radius that is either set to the dust sublimation radius (R_{sub}) or varied between R_{sub} and $1000 R_{\text{sub}}$.

The T. P. Robitaille (2017) SED model grid used in this work includes: stellar radius = $0.1\text{--}100 R_{\odot}$, stellar temperature = $2000\text{--}30,000$ K, disk mass = $10^{-8}\text{--}10^{-1} M_{\odot}$, outer disk radius = $50\text{--}5000$ au, envelope density = $10^{-24}\text{--}10^{-16} \text{ g cm}^{-3}$, envelope power-law index of -2 to -1 , cavity density = $10^{-23}\text{--}10^{-20} \text{ g cm}^{-3}$, and cavity opening angle = $0^{\circ}\text{--}60^{\circ}$.

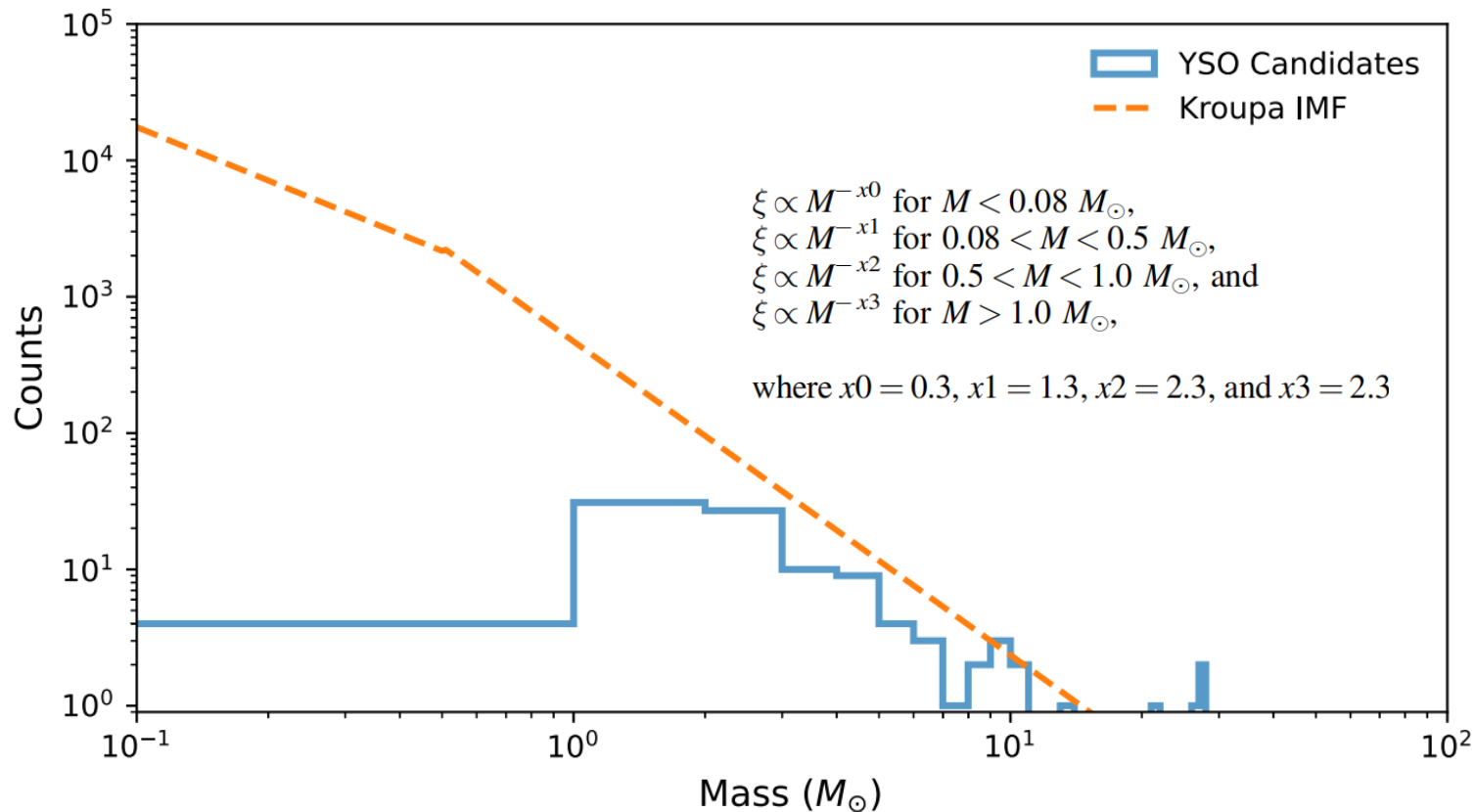


Figure 6. Kroupa IMF fit to the mass distribution of the 102 YSO candidates. The total YSO mass is $1965 M_{\odot}$. Assuming a typical formation time of 10^5 yr, the resulting SFR is $0.02 M_{\odot} \text{ yr}^{-1}$.

Carlson et al. (2012) study nine different star-forming regions in the LMC and assume a typical formation timescale of 10^6 yr when calculating the SFR in each region. When scaling their SFR to 10^5 yr, the resulting SFR ranges from $0.008 M_{\odot} \text{ yr}^{-1}$ in N144 to $0.068 M_{\odot} \text{ yr}^{-1}$ in N160. Other high-mass star-forming regions in the LMC have gone through multiple episodes of star formation. In contrast, H72.97-69.39 is going through its first starburst phase (B. B. Ochsendorf et al. 2017). Due to the intense luminosity and high concentration of YSO candidates, Ochsendorf et al. (2017) labeled this source as a proto-SSC candidate still ramping up its YSO production.

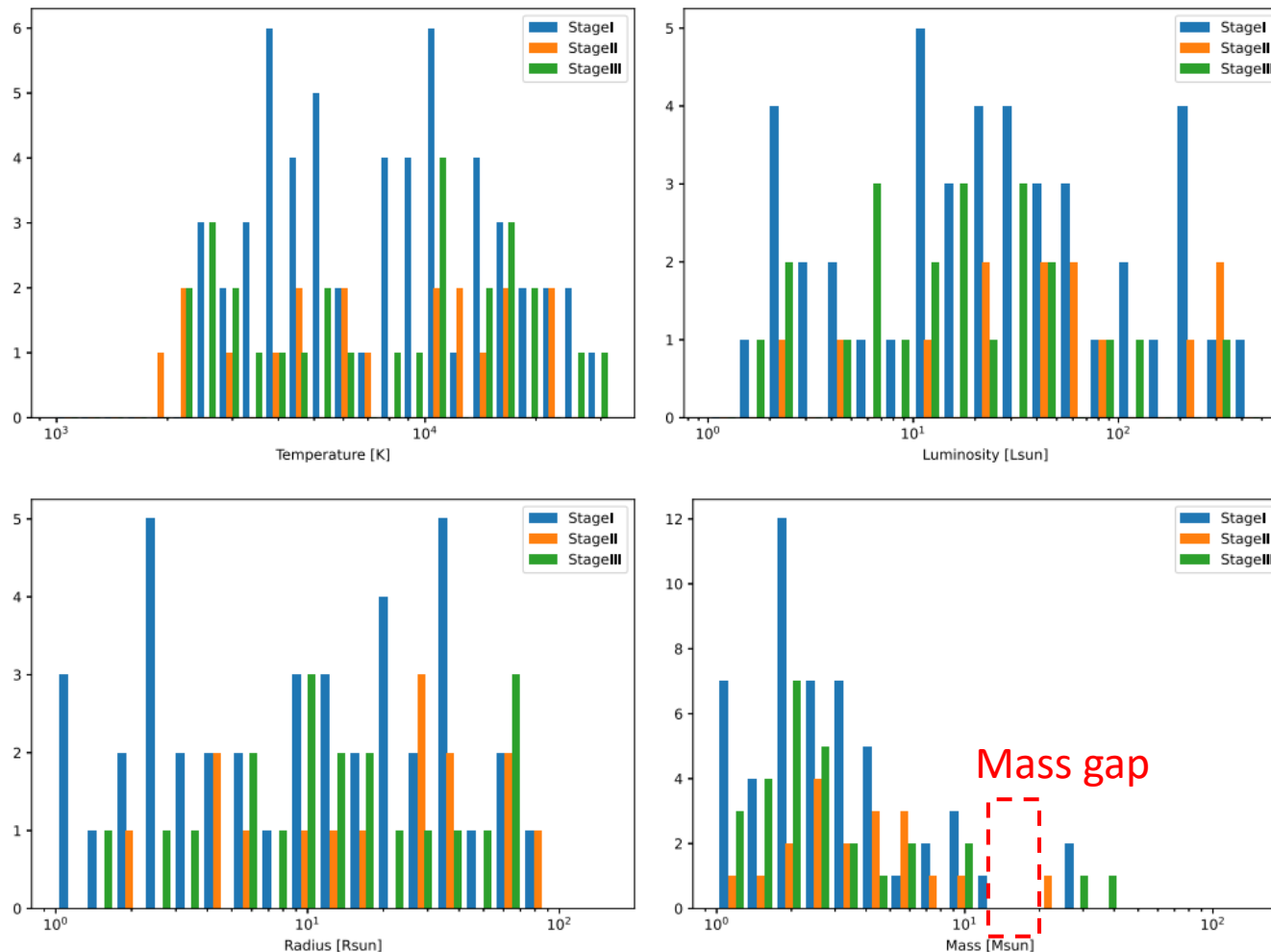


Figure 4. Top left: effective temperature histogram of the five spectroscopically confirmed YSOs and 97 YSO candidates in this work. Top right: luminosity histogram of the YSO candidates. Bottom left: stellar radius histogram of the YSO candidates. Bottom right: mass histogram of the YSO candidates.

YSO candidates

Temperature range: 2040 - 28,700 K

Luminosity range: 0.4–581,468 L_{\odot}

Mass range: 0.7–40 M_{\odot}

The observed gap in stellar mass not due to fitting constraints or methodology

Indeed, MIRI images cover all the central region of H72.97- 69.39, and MIRI/Medium Resolution Spectroscopy instrument IFU observations (flux density integration -> photometry extraction) cover the saturated region. This gives a complete inventory of the massive YSOs greater than 8 M_{\odot} in the MIRI footprint.

The observed gap can possibly be explained by different formation mechanisms taking place for massive YSO candidates with masses greater than 20 M_{\odot} versus massive YSO candidates with masses 8–13.5 M_{\odot} .

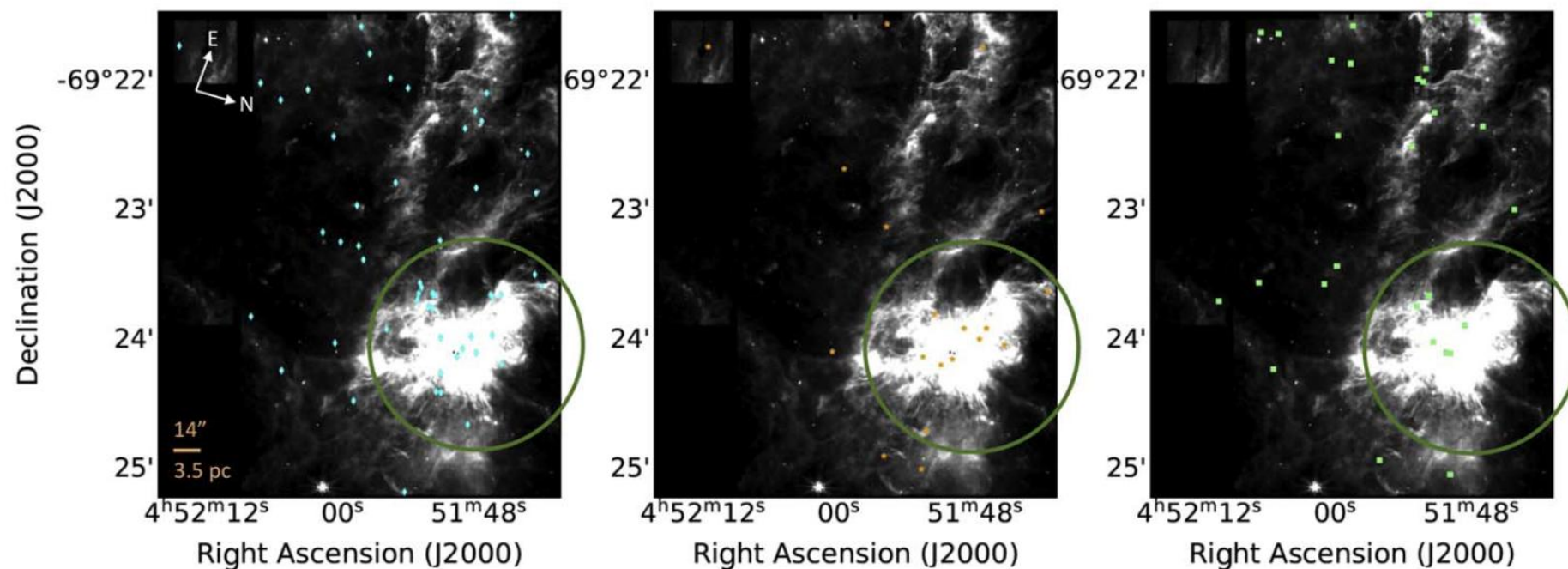
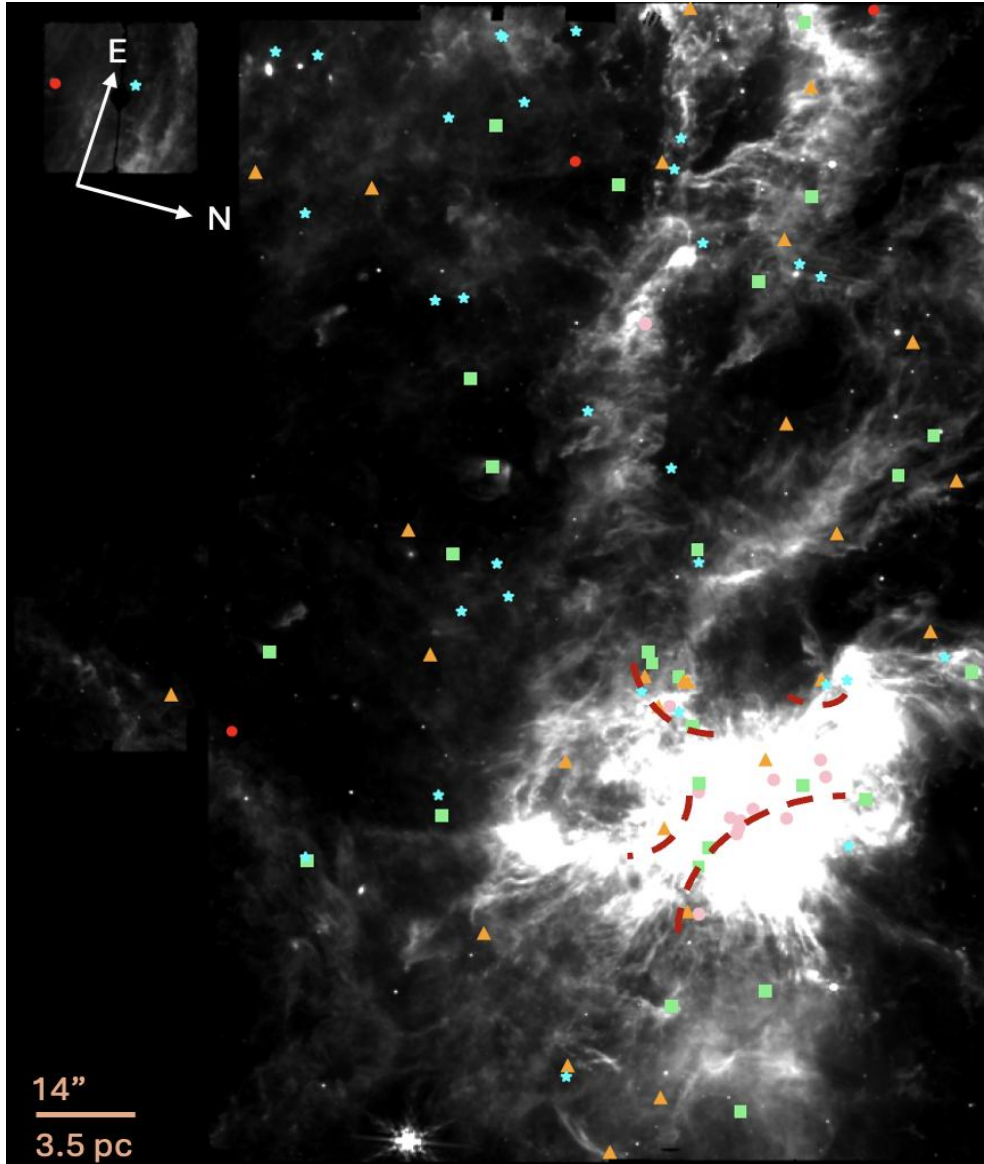


Figure 5. We plot the five YSOs and 97 YSO candidates separated by evolutionary stage on the MIRI F1000W wavelength image. Left: 55 Stage I YSO candidates. Center: 19 Stage II YSO candidates. Right: 28 Stage III YSO candidates. We overlay a green circle with radius $59''$ (14.8 pc) within which 70% of the YSO mass is contained.

Tan (2000) find cloud–cloud collisions can lead to compressed, high-density, localized regions within the clouds. Such compressed and high-density regions have been observed to be associated with the central five protostars of H72.97-69.39. O. Nayak et al. (2019) find gas tracers HCN, HCO⁺, and SO, with densities 10^5 – 10^6 cm⁻³. If these dense regions are magnetically supercritical, they can collapse rapidly to form high-mass OB stars as well as low-mass stars. A triggering event such as two filamentary molecular clouds colliding could explain the observed mass gap: the very high-mass stars greater than 20 M formed via filamentary collision, in which high density gas necessary for high-mass star formation can form. The eight other massive YSO candidates in H72.97-69.39 could have formed through local gravitational collapse, as shown in simulations by F. Heitsch et al. (2008). The two different formation mechanisms can possibly be the reason for the observed mass gap for massive YSOs in H72.97-69.39.

Embedded Young Stellar objects near H72.97-69.39: A Forming SSC in N79



There are 4 YSOs less than $1 M_{\odot}$, 31 between $1-2 M_{\odot}$, 27 between $2-3 M_{\odot}$, 27 between $3-8 M_{\odot}$, and 13 greater than $8 M_{\odot}$ shown in this F1000W MIRI image. 12/13 YSOs greater than $8 M_{\odot}$ are located at or near the super star cluster H72.97-69.39.

More massive YSOs seem to be forming along shell-like arcs closer to the gravitational center of the cluster, and less massive YSOs form further away and in pillar-like structures. The mass segregation observed with MIRI is similar to observations of RCW120 (Figueira et al. 2017) and modeling done by Walch et al. (2013)

The majority of the low mass stars are located outside the 14.8 pc radius and scattered along the filamentary-like structure seen in F1000W. It is likely we are seeing an interplay of high-mass stars forming quickly near the gravitational center of this cluster and low-mass stars forming within low-mass clumpy molecular gas spread far apart from one another. Observations of young stellar clusters NGC 1818, NGC 2004, NGC 2100, and NGC 330 in the Magellanic Clouds show evidence of more massive stars being more centrally located within a cluster, and that this phenomenon is set during the formation period of a cluster.

Tailo et al. 2020

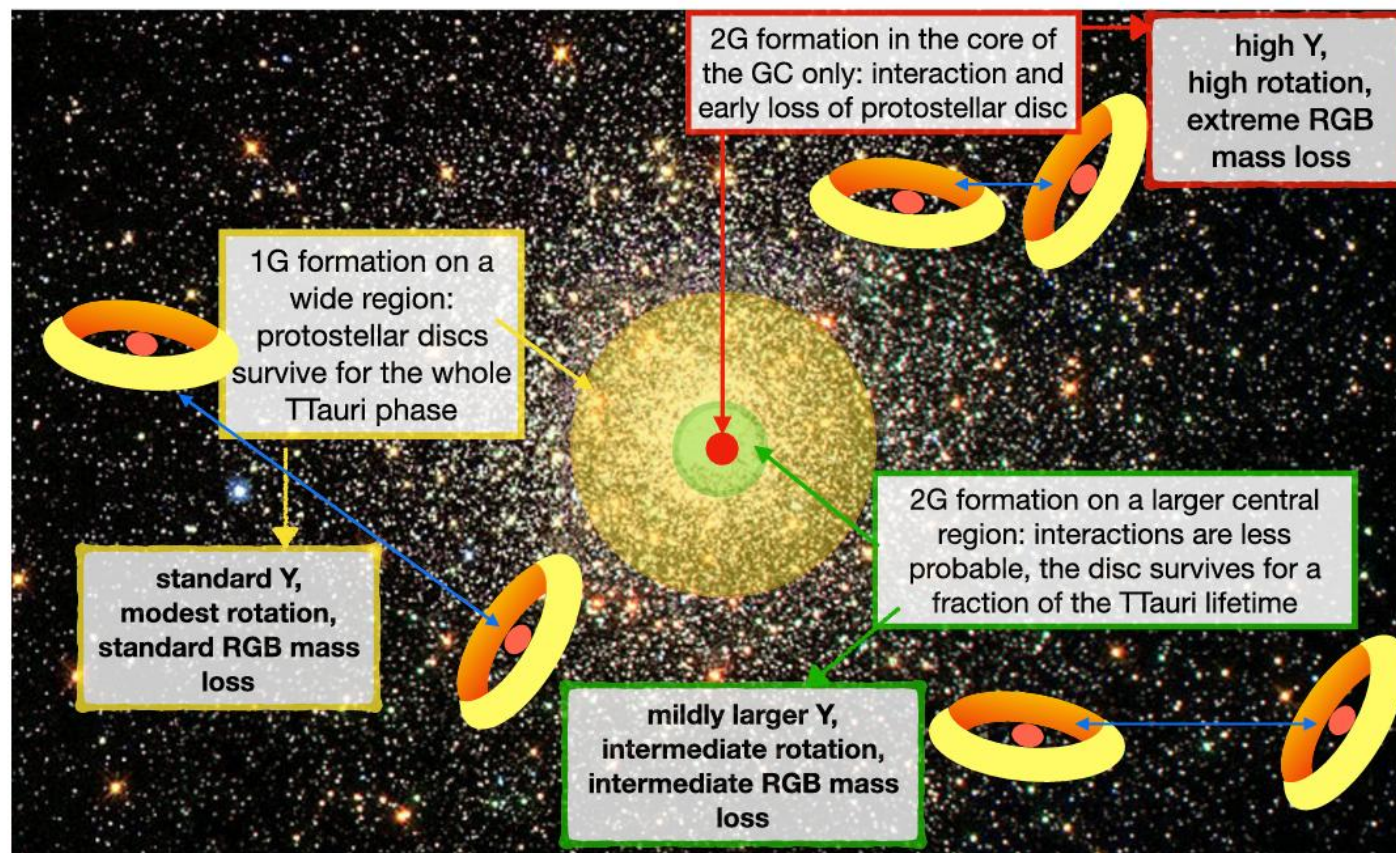


Figure 18. Schematic interpretation of the different rotation of 1G and 2G stars. During the pre-main-sequence evolution, the rotation of the central contracting star is magnetically locked to the rotation of its residual accretion disc, having a diameter of 50–100 au. While the 1G formation occurs in an ambient of moderate density (yellow region), where the disc–disc interactions occur on a time-scale longer than the typical stellar contraction time (few 10^6 yr), the 2G formation occurs in much smaller central regions (green and red regions, representing less and more extreme 2G populations; these regions represent either star formation in the same cluster at successive times, or star formation in clusters of different initial mass), where collisions and an early loss of the accretion disc are much more probable. Free stellar contraction and increase of the rotation rate follow the loss of the disc. Rapidly rotating cores delay ignition of the core-helium flash and allow a larger RGB mass-loss. This scheme, supported by hydrodynamical simulations, is at the basis of the direct correlation between the extra-mass-loss, the helium overabundance of the 2Ge populations, and the total initial mass of the cluster.